CHEMISTRY OF MATERIALS
Article

Chem. Mater. **2010,** *22,* 2203–2212 2203
DOI:10.1021/cm902300q

Synthesis, Characterization, Defect Chemistry, and FET Properties of Microwave-Derived Nanoscaled Zinc Oxide

Jörg. J. Schneider,*[,†] Rudolf C. Hoffmann,[†] Jörg Engstler,[†] Andreas Klyszcz,[‡] Emre Erdem,[§] Peter Jakes,[§] Rüdiger-A. Eichel,[§] Luciana Pitta-Bauermann,[⊥] and Joachim Bill[⊥]

[†]*Fachbereich Chemie, Eduard Zintl-Institut, Anorganische Chemie, TU Darmstadt, Petersenstrasse 18, 64287 Darmstadt, Germany,* [‡]*Merck KGaA, Frankfurter Strasse 250, 64293 Darmstadt, Germany,* [§]*Institut für Physikalische Chemie I, Albert-Ludwigs Universität Freiburg, Albertstrasse 21, 79106 Freiburg, Germany, and* [⊥]*Institut für Materialwissenschaft der Universität Stuttgart, Max-Planck-Institut für Metallforschung, Heisenbergstrasse 3, 70569 Stuttgart, Germany*

Received July 27, 2009. Revised Manuscript Received February 16, 2010

The formation of nanoscale zinc oxide particles with an almost-monomodal size distribution synthesized by microwave heating of solutions of mononuclear zinc oximato or zinc acetylacetonato complexes in various alkoxyethanols is investigated. Transparent stable suspensions that contain these particles can be obtained from the zinc oximato precursor. Based on electron paramagnetic resonance (EPR) studies, a core/shell model with a finite surface shell thickness of 1.000 ± 0.025 nm is proposed for the ZnO nanoparticles. Field-effect transistor (FET) devices with these ZnO particles as the active semiconducting layer exhibited a charge carrier mobility of 0.045 $cm^2/(V\ s)$ and $I_{on/off}$ current ratios of ~460.000, with a threshold voltage of 8.78 V.

Introduction

The electronic properties of ZnO can be tuned from an insulating ceramic over semiconducting to complete metallic behavior.[1−4] In this respect, it is of utmost importance to understand the defect chemistry[5] of solution-processed size-selective nanoscale ZnO nanoparticles in more detail, because thin films of this material have unique performance properties in materials printing technology and a high application potential as active semiconductor in thin-film transistors (TFTs).[6−19] However, for such an in-depth understanding and future application of ZnO in functional devices (e.g., TFTs), a systematic investigation and understanding of the morphology of such particles is desperately needed. Therefore, the synthesis of equisized, uniform, and well-dispersible ceramic particles in the size regime of 10−100 nanometers in reasonable yields is a materials chemistry challenge.[20] Nanoparticles are readily available from gas-phase reactions; however, for processing from solution, a subsequent dispersion step is required in this case.[17,18] Thus, the formation of particles in solution, whereby stable dispersions are obtained, is preferred. Particles with a narrow size distribution can be synthesized in hydrolytic reactions by allowing only a slight supersaturation using a large dilution of the reaction mixture and

*Author to whom correspondence should be addressed. Fax: +49-6151-163470. E-mail: joerg.schneider@ac.chemie.tu-darmstadt.de.

(1) Fortunato, E.; Gonçalves, A.; Pimentel, A.; Barquinha, P.; Gonçalves, G.; Pereira, L.; Ferreira, I.; Martins, R. *Appl. Phys. A* **2009**, *96*, 197–205.
(2) Martins, R.; Barquinha, P.; Pimentel, A.; Pereira, L.; Fortunato, E.; Kang, D.; Song, I.; Kim, C.; Park, C.; Park, Y. *Thin Solid Films* **2008**, *516*, 1322–1325.
(3) Pearton, S. J.; Norton, D. P.; Ip, K.; Heo, Y. W.; Steiner, T. *J. Vac. Sci. Technol., B* **2004**, *22*, 932–948.
(4) Özgür, Ü.; Alivov, Y. I.; Liu, C.; Teke, A.; Reshchikov, M. A.; Dogan, S.; Avrutin, V.; Cho, S. J.; Morkoç, H. *J. Appl. Phys.* **2005**, *98*, 041301.
(5) McCluskey, M. D.; Jokela, S. J. *J. Appl. Phys.* **2009**, *106*, 071101.
(6) Schneider, J. J.; Hoffmann, R. C.; Engstler, J.; Soffke, O.; Jaegermann, W.; Issanin, A.; Klyszcz, A. *Adv. Mater.* **2008**, *20*, 3383–3387.
(7) Schneider, J. J.; Hoffmann, R. C.; Engstler, J.; Dilfer, S.; Klyszcz, A.; Erdem, E.; Jakes, P.; Eichel, R. A. *J. Mater. Chem.* **2009**, *19*, 1449–1457.
(8) Li, C. S.; Li., Y. N.; Wu, Y. L.; Ong, B. S.; Loutfy, R. O. *J. Mater. Chem.* **2009**, *19*, 1626–1634.
(9) Li, C. S.; Li., Y. N.; Wu, Y. L.; Ong, B. S.; Loutfy, R. O. *J. Phys. D: Appl. Phys.* **2008**, *41*, 125102.
(10) Pal, B. N.; Trottman, P.; Sun, J.; Katz, H. E. *Adv. Funct. Mater.* **2008**, *18*, 1832–1839.
(11) Cheng, H. C.; Chen, C. F.; Tsay, C. Y. *Appl. Phys. Lett.* **2007**, *90*, 012113.
(12) Cheng, H. C.; Chen, C. F.; Tsay, C. Y.; Leu, J. P. *J. Alloys Compd.* **2009**, *475*, L46–L49.
(13) Yang, C. W.; Hong, K. Y.; Jang, J. Y.; Chung, D. S.; An, T. K.; Choi, W. S.; Park, C. E. *Nanotechnology* **2009**, *20*, 465201.
(14) Noh, Y. Y.; Cheng, X. Y.; Sirringhaus, H.; Sohn, J. I.; Welland, M. E.; Kang, D. J. *Appl. Phys. Lett.* **2007**, *91*, 043109.
(15) Faber, H.; Burkhardt, M.; Jedaa, A.; Kälblein, D.; Klauk, H.; Halik, M. *Adv. Mater.* **2009**, *21*, 3099–3104.
(16) Oh, J. Y.; Park, J. H.; Kang, S. Y.; Hwang, C. S.; Shim, H. K. *Chem. Commun.* **2009**, 4545–4547.
(17) Okamura, K.; Mechau, N.; Nikolova, D.; Hahn, H. *Appl. Phys. Lett.* **2008**, *93*, 083105.
(18) Bubel, S.; Nikolova, D.; Mechau, N.; Hahn, H. *J. Appl. Phys.* **2009**, *105*, 064514.
(19) Richter, T. V.; Stelzl, F.; Schulz-Gericke, J.; Kerscher, B.; Würfel, U.; Niggemann, M.; Ludwigs, S. *J. Mater. Chem.* **2010**, *20*, 874–879.
(20) Burda, C.; Chen, X. B.; Narayanan, R.; El-Sayeed, M. A. *Chem. Rev.* **2005**, *105*, 1025–1102.

Published on Web 03/05/2010

Scheme 1. Structure of the Precursors (1) Zinc Acetylacetonate and (2) Zinc Oximate

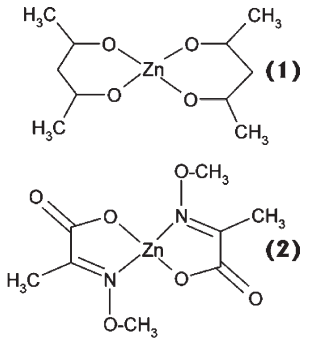

extended reaction times.[21,22] Nonhydrolytic reactions were suggested as alternatives, because the condensation typically can be controlled more easily.[23,24] Another frequently applied route is the oxidative decomposition of organometallic precursors, which has the advantage of yielding pure compounds, but it requires proper handling of air- and moisture-sensitive compounds.[25,26]

The employment of microwave heating offers a further interesting method for controlling the reaction process for ZnO nanoscale particles. Synthetic procedures that make use of the single-source precursor concept in which a single zinc compound is used as a precursor to ZnO, avoiding any additional reaction steps besides the decomposition to ZnO, and, thus, minimizing contaminations are especially valuable.[27−33] This is important, with respect to further processing to thin films in electronic applications. The choice of such alternative ZnO precusors would be advantageous for this technique, because the widely used zinc acetate did not lead to phase-pure ZnO.[29,31,32]

In this work, we report the formation of ZnO nanoparticles of discrete sizes derived from zinc acetylacetonate and zinc oximato complexes (see Scheme 1) by microwave heating in different alkoxyethanols. The present study shows that particle morphology and aggregation, as well as the defect chemistry, is strongly dependent on the precursor type. Different types of defects could be identified by means of photoluminescence (PL) and electron paramagnetic resonance spectroscopy (EPR). Finally a field-effect transistor (FET) was built using ZnO nanoparticles derived from the single-source precursor as an active device semiconductor.

Experimental Section

Reagents. Zinc acetylacetonate monohydrate (99.99%, Aldrich), methoxyethanol, ethoxyethanol, and *n*-butoxyethanol were used as purchased. Zinc oximate dihydrate was synthesized according to the procedure from Hill et al.[34] and recrystallized twice from water. The sodium content of zinc oximate was <100 ppm, according to inductively coupled−plasma mass-spectrometry (ICP-MS).

Particle Synthesis. The required amount of the precursor was dissolved in an alkoxyethanol (methoxyethanol, ethoxyethanol, or *n*-butoxyethanol), giving a total of 10 g. Concentrations for the precursors were in the range of 2.5−10 wt %, corresponding to 10.0−37.5 mol % of (**1**) or 7.5−30.0 mol % for (**2**), respectively. The solution was pressed through a syringe filter (Millipore, 200 nm) and filled in a Teflon vessel (Savillex, 120 mL in volume, 50 mm in diameter; maximum overpressure = 5−6 bar).

Heating was performed in a conventional kitchen microwave (800 W, 4 min). Suspensions derived from oximate were investigated without further dilution, whereas those derived from acetylacetonate were diluted with further solvent (1:9, v:v). Particles could be isolated by flocculation from the suspensions with water and subsequent centrifugation. The particles were then washed with acetone and distilled water and dried at 75 °C in air.

Particle Characterization. Dynamic light scattering (DLS) is performed using Zetasizer Nano equipment (Malvern). Samples were measured in 10-mm quartz cuvettes. Data evaluation was performed with the software supplied by the manufacturer, according to ISO 13321 and ISO 22412 standards, employing a Gaussian particle size distribution (with a standard deviation of σ). Cumulative analysis of the autocorrelation function yields an average value z for the hydrodynamic radius and the polydispersity index (PI = σ^2/z^2), as a characteristic for the size distribution. The polydispersity index (values for all samples were 0.05−0.20) was in accordance with the assumed monomodal size distribution and did not show an obvious dependence from the median particle diameter.

Brunauer−Emmett−Teller (BET) surface area analysis is performed using a NovaWin2 system (Quantachrome). Scanning electron microscopy (SEM) is performed with a Philips Model XL 30 FEG system (20 kV); samples were spin-coated on silicon slides, and no further coating with metal was applied. Transmission electron microscopy (TEM) was performed (Tecnai G2 F20 (FEI), 200 kV), using samples on a lacey-carbon copper grid (300 mesh). X-ray diffraction (XRD) was conducted using a STOE Model Stadi-P system (Cu Al Kα radiation). Thermogravimetry (TG) analysis was performed using a Netzsch Model TG209N1 system; samples were heated in aluminum oxide crucibles at a rate of 10 K/min in oxygen. Infrared (IR) spectroscopy (Bruker, Model Vector 22) and photoluminescence (PL) (Horiba, Model Fluorolog-3) studies were conducted; the excitation wavelength was 325 nm. Electron paramagnetic resonance (EPR) analysis was applied; X-band (9.31 GHz) continuous-wave EPR measurements were made on a Bruker spectrometer. The magnetic field was determined using a nuclear magnetic resonance gaussmeter (ER 035M, Bruker),

(21) Spanhel, L. *J. Sol−Gel Sci. Technol.* **2006**, *39*, 7–24.
(22) Weller, H. *Philos. Trans. R. Soc. London, A* **2003**, *361*, 229–239.
(23) Pinna, N.; Niederberger, M. *Angew. Chem., Int. Ed.* **2008**, *47*, 5292–5304.
(24) Garnweitner, G.; Niederberger, M. *J. Mater. Chem.* **2008**, *18*, 1171–1182.
(25) Kahn, M.; Chaudret, B. *J. Mater. Chem.* **2009**, *19*, 4044–4060.
(26) Carnes, C. L.; Klabunde, K. J. *Langmuir* **2000**, *16*, 3764–3772.
(27) Gerbec, J. A.; Magana, D.; Washington, A.; Strouse, G. F. *J. Am. Chem. Soc.* **2005**, *127*, 15791–15800.
(28) Groisman, Y.; Gedanken, A. *J. Phys. Chem. C* **2008**, *112*, 8802–8808.
(29) Bhattacharyya, S.; Gedanken, A. *J. Phys. Chem. C* **2008**, *112*, 659–665.
(30) Hu, X. L.; Gong, J. M.; Zhang, L. Z.; Yu, J. C. *Adv. Mater.* **2008**, *20*, 4845–4850.
(31) Bilecka, I.; Elser, P.; Niederberger, M. *ACS Nano* **2009**, *3*, 467–477.
(32) Bilecka, I.; Djerdj, I.; Niederberger, M. *Chem. Commun.* **2008**, 886–888.
(33) Liu, J. F.; Bei, Y. Y.; Wu, H. P.; Shen, D.; Gong, J. Z.; Li, X. G.; Wang, Y. W.; Jiang, N. P.; Jiang, J. Z. *Mater. Lett.* **2007**, *61*, 2837–2840.
(34) Hill, M. R.; Jones, A. W.; Russell, J. J.; Roberts, N. K.; Lamb, R. N. *Inorg. Chim. Acta* **2005**, *358*, 201–206.

and, as a standard field marker, polycrystalline DPPH with $g = 2.0036$ was used for the exact determination of the magnetic field offset.

FET Characterization. Substrates for FET devices consisted of highly *n*-doped silicon with a 90-nm-thick layer of SiO_2, on which gold electrodes were attached with an intermediate adhesive layer of indium tin oxide (ITO). The electrodes possessed an interdigital structure with a channel width (W) of 10 mm and a channel length (L) of 20 μm. The ceramic layer was brought up by spin-coating (2000 rpm) a dispersion obtained from the microwave reaction of 5 wt % of **2** in methoxyethanol and the removal of $\sim^2/_3$ of the solvent under reduced pressure. Afterward, the entire FET substrate was calcined in argon at 250 °C for 10 min, followed by 325 °C for 1 min. Alternatively, the FET device was subjected to ultraviolet (UV) irradiation (UVACUBE 2000 (Dr. Hönle AG, UV Technology), 200 mW/cm^2, iron−mercury lamp) for 2 min under ambient conditions and afterward heated at 200 °C for 1 min in argon. Electrical characterization was conducted with a semiconductor parameter analyzer (Agilent, Model HP 4155A) in a glovebox under argon atmosphere.

To extract the carrier charge mobility from the transistor characteristics, the square root of the drain current was plotted versus the gate-to-source voltage, yielding a straight line in the saturation region. Linear regression was applied to fit this part of the transfer characteristic to a straight line yielding the slope and the intersection with the abscissa. The mobility was then extracted from the slope of the curve. In addition, the intersection point can be used to determine the threshold voltage of the device. The full extraction procedure has been described earlier in detail.[6]

Results and Discussion

Particle Synthesis. Zinc oxide particles were obtained via the microwave heating of solutions of the precursors zinc oximato or acetylacetonato, respectively in different alkoxyethanols ($RO-C_2H_4OH$) in closed Teflon vessels. (For $R = CH_3$, C_2H_5, and n-C_4H_9 boiling points at ambient pressure are reported as 124 °C, 135, and 169 °C, respectively.[35]) The bis-acetylacetonato precursor **1** yielded whitish turbid suspensions. These exhibited complete sedimentation within 24−48 h. However, suspensions obtained from the bis-oximato complex **2** were transparent (see Figure 1 of the Supporting Information). No obvious sedimentation from these suspensions was observed within several months. The use of sufficiently pure precursor material was important, because the presence of higher amounts of alkali ions leads to flocculation or sedimentation.[36,37] Flocculation was also observed via the addition of distilled water to the organic solvent.[36] This effect could be used purposely to facilitate centrifugation and separation of the ceramic ZnO nanoparticles from the suspension.

Attempts were made to increase the solids loading of the suspensions obtained from **2**. Because the ceramic yield of the precursor is ~25 wt %, the solids content of the slurries was < 2.5 wt % zinc oxide. However, it was possible to remove part of the solvent with a rotary evaporation at $T = 60$ °C and a reduced pressure of ~25−50 mbar in the case of methoxy- and ethoxyethanol. No flocculation or sedimentation was observed then, and the suspensions remained stable over several weeks.

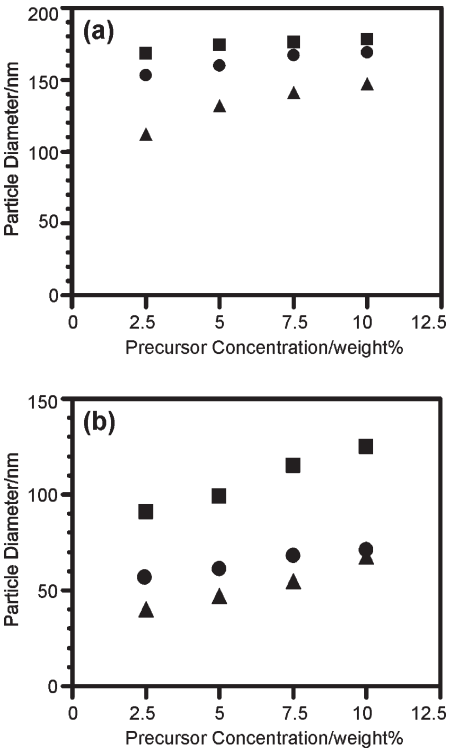

Figure 1. Particle diameter (from DLS) of ZnO particles obtained from (a) the zinc acetylacetonato complex **1** and (b) the zinc oximato complex **2** in different suspensions of alkoxyethanols ((▲) methoxyethanol, (●) ethoxyethanol, and (■) *n*-butoxyethanol).

Particle Size and Morphology. The size of the particles was determined by dynamic light scattering (DLS). Results for solutions obtained from **1** and **2** are shown in Figures 1a and 1b, respectively. Higher precursor concentrations of **1** and **2** led to larger particles, whereby this effect was more pronounced for particles from the oximato complex than for those from the acetylacetonato complex. The choice of the solvent had a larger influence on the particle sizes, whereby reaction in a solvent with a higher boiling point led to larger particle sizes. In all cases, the mean diameter (as determined by DLS) remained constant, even over longer periods of time (i.e., several weeks), suggesting that the observed particles did not show fragmentation into smaller entities.

The specific surface of powders isolated from the aforementioned suspenions in ethoxyethanol were determined from the Brunauer−Emmett−Teller (BET) absorption isotherms (see Figure 2). As expected from the DLS measurements, the specific surface was larger for powders obtained from **2** than those from **1**. In both cases, no simple linear dependence of the specific surface from the precursor concentration was observed. For powders obtained from **1**, the specific surface increased with lower precursor concentrations. For ZnO powders obtained from precursor **2**, however, the curve exhibited a maximum. This effect might be explained by the different

(35) *Handbook of Chemistry and Physics, Student Edition*, Vol. *1*; CRC Press: Boca Raton, FL, 1988.
(36) Sigmund, W. M.; Bell, N. S.; Bergström, L. *J. Am. Ceram. Soc.* **2000**, *83*, 1557–1574.
(37) Widegren, L.; Bergström, L. *J. Am. Ceram. Soc.* **2002**, *85*, 523–528.

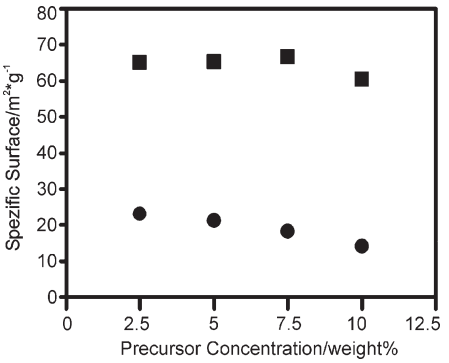

Figure 2. Specific surface according to BET absorption isotherms of particles from **1** (circles) or complex **2**(squares) in ethoxyethanol.

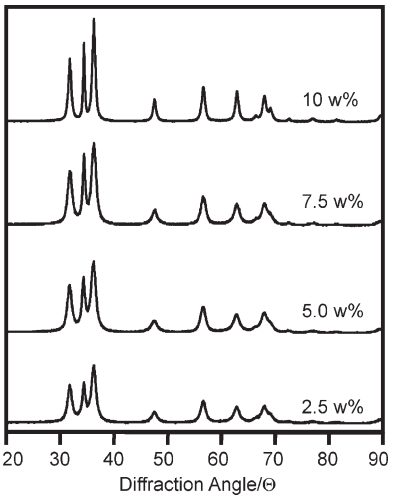

Figure 3. XRD diagrams of particles from the decomposition of **1** in ethoxyethanol for various concentrations.

contents of fines or by variation of the particle shape (i.e., significant deviation of the particles from an ideal spherical form).

The morphology of the particles was investigated by means of scanning electron microscopy SEM (see Figures 2 and 3 of the Supporting Information). For both precursors, no significant formation of hard agglomerates or intergrowth of individual particles was observed. Particles appeared well-separated and uniform. The size from the SEM micrographs are in full aggrement with the DLS measurements. SEM was also used to characterize particles from slurries after removal of the solvent by destillation under reduced pressure. The micrographs confirmed that no larger aggregates were formed (see Figure 4 of Supporting Information).

For the identification of crystalline phases, X-ray diffraction (XRD) measurements were performed (see Figures 3 and 4). All samples investigated here solely exhibited reflections of nanocrystalline zincite. No other phases could be detected. A Rietveld analysis was used to determine the crystallite sizes for the first three reflections (see Tables 1 and 2). As a result, higher precursor concentrations led to larger crystallite sizes. For both precursors, an elongation in the direction of the *c*-axis (i.e., perpendicular to the (002) plane) was observed.

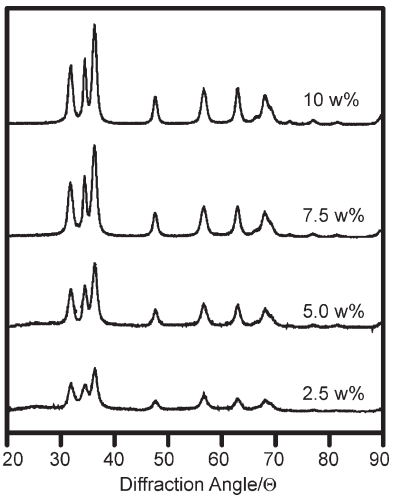

Figure 4. XRD diagrams of particles from the decomposition of **2** in ethoxyethanol for various concentrations.

Table 1. Average Crystallite Sizes Calculated from the Width of Selected Reflections Corresponding to Figure 3 (Precursor 1)

precursor concentration (wt %)	Average Crystallite Size (nm)		
	(100)	(002)	(101)
10	15.9	31.8	16.5
7.5	10.2	18.2	10.0
5.0	10.0	13.7	9.4
2.5	9.4	12.1	9.5

Table 2. Average Crystallite Sizes Calculated from the Width of Selected Reflections Corresponding to Figure 4 (Precursor 2)

precursor concentration (wt %)	Average Crystallite Size (nm)		
	(100)	(002)	(101)
10	11.2	17.7	12.1
7.5	9.8	15.2	11.0
5.0	9.5	12.5	9.8
2.5	8.6	11.1	9.2

However, the crystallite sizes from XRD were drastically smaller than expected from the DLS and SEM measurements. Therefore, high-resolution transmission electron microscopy (HRTEM) was used to reveal the structural composition of the ZnO particles (see Figures 5 and 6). The particles show a uniform appearance and were assembled of smaller crystallites (descriptively denoted as the "blackberry structure" in previous publications). ZnO specimens obtained from precursor **1** were almost spherical, whereas those from precursor **2** exhibited a mandrel or pyramidal shape.

Wang et al. were able to obtain non-agglomerated, almost-spherical zinc oxide particles from zinc oximato complexes in amines by thermal decomposition. The sizes were in the range of 4−6 nm, increasing while the synthesis temperature was increased from 130 °C to 230 °C.[38] Niederberger et al. could obtain inconsistently large agglomerates that are composed of crystallites of zinc oxide from **1** in benzylalcohol. Crystallite sizes were reported to be above 20 nm, whereby the evident elongation in direction

(38) Wang, Y. S.; Thomas, P. J.; O'Brien, P. *J. Phys. Chem. B* **2006**, *110*, 4099–4104.

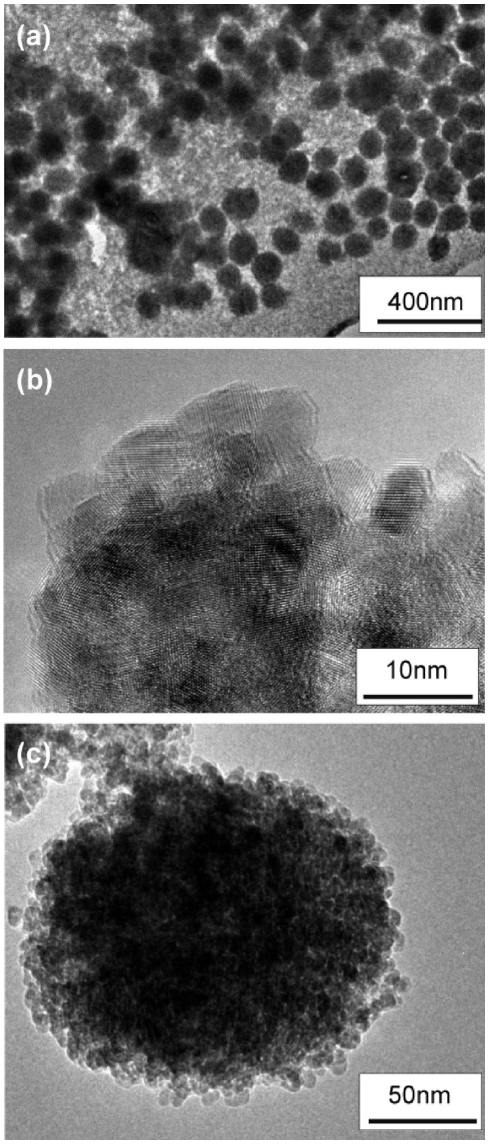

Figure 5. HRTEM images of powders obtained from precursor **1** (5 wt %) in ethoxyethanol.

of the *c*-axis was not investigated in detail.[32] However, the reaction of **1** in oleylamine leads to mandrel-shaped, not agglomerated, crystallites, with sizes in the range of 7−11 nm.[33]

Further investigations were concerned with the contents of organic residues on the particles. Thermogravimetric (TG) analysis of powders obtained from **1** showed a continuous weight loss of 200°−400 °C (see Figure 7a). In ZnO specimens obtained from **2**, a first distinct step was observed at 200 °C, followed by further loss at a temperature of 400 °C (Figure 7b). In both cases, however, all volatile residues were removed at ∼400 °C and no further weight loss was observed thereafter, indicating the complete formation of ZnO at that temperature.

Infrared (IR) spectroscopy of as-isolated ZnO particles (i.e., without further heat treatment at elevated temperatures) exhibted many signals for both precursor compounds **1** and **2** (see Figures 8 and 9, respectively). These clearly did not originate from the solvent, in which the reaction was executed, but they were related to several

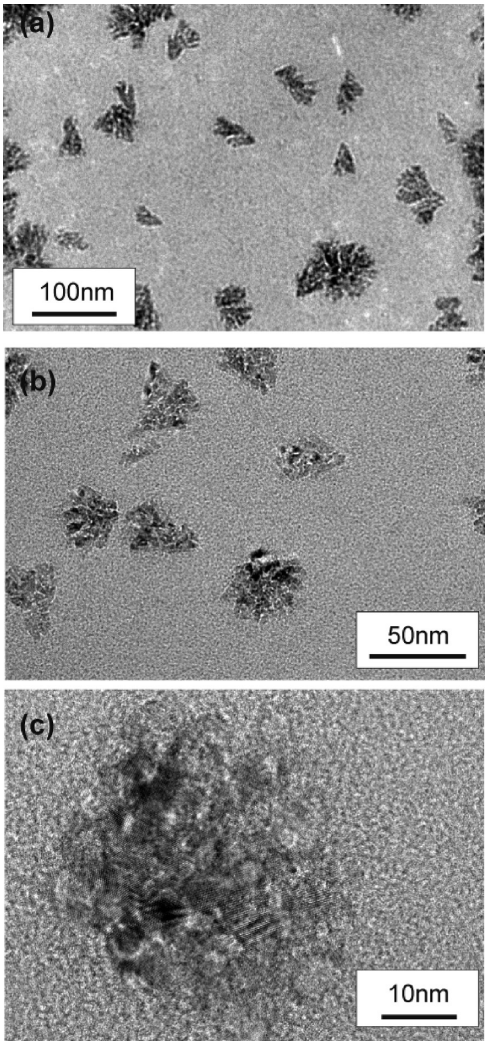

Figure 6. HRTEM images of powders obtained from precursor **2** (5 wt %) in ethoxyethanol.

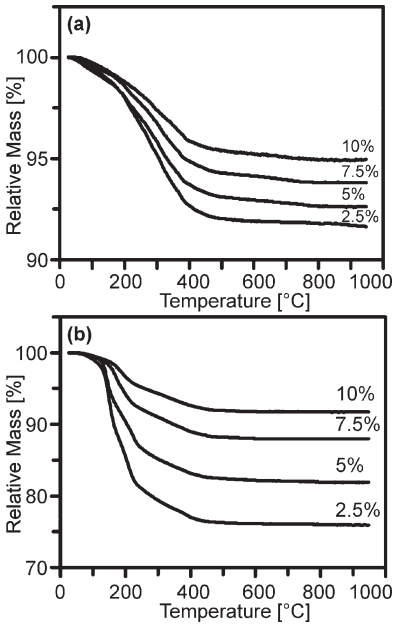

Figure 7. Thermogravimetric (TG) loss curve determined in oxygen of ZnO nanopowders obtained from (a) **1** and (b) **2**.

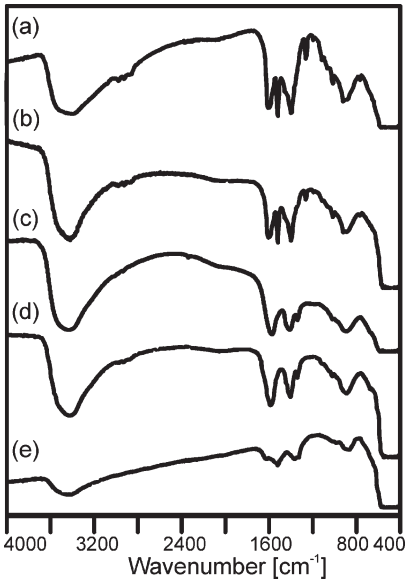

Figure 8. IR spectra of powders from the decomposition of 10 wt % of **1** in ethoxyethanol: as-prepared powder (spectrum a), as well as after further calcination at 150 °C (spectrum b), 250 °C (spectrum c), 350 °C (spectrum d), and 500 °C (spectrum e).

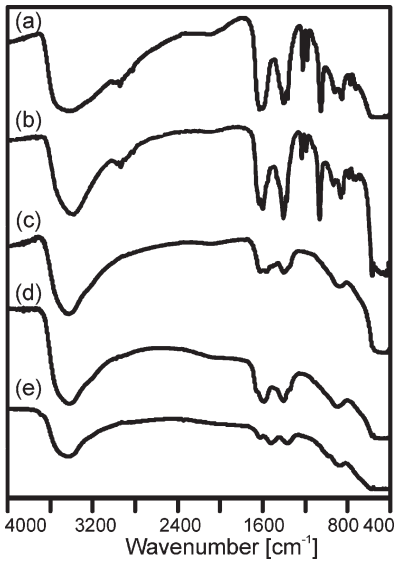

Figure 9. IR spectra of powders from the decomposition of 10 wt % of **2** in ethoxyethanol: as-prepared powder (spectrum a), as well as after further calcination at 150 °C (spectrum b), 250 °C (spectrum c), 350 °C (spectrum d), and 500 °C (spectrum e).

functional groups present within the starting precursor molecules.[7,31] Signals at 1603 and 1410 cm^{-1} in both types of samples might be attributed to the antisymmetric ν_{asym} and symmetric ν_{sym} valence vibration of carboxylate groups.[39,40]

All of the original signals were still present after calcination at 150 °C, but they disappeared at temperatures of >250 °C. After heat treatment at elevated temperatures, only vibration bands corresponding to nanoscale zinc oxide including surface hydroxylation were observed.

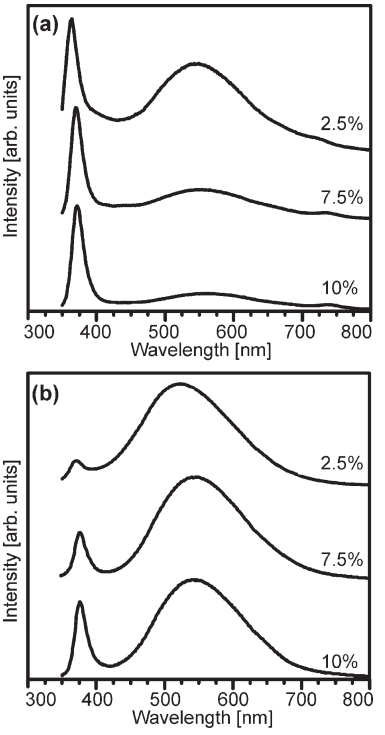

Figure 10. PL spectra of powders obtained from (a) **2** and (b) **1** in ethoxyethanol.

The broad absorption at 3400−3600 cm^{-1} corresponds to the O−H stretching vibrations and is accompanied by in-plane deformation vibrations ~1610 cm^{-1}.[41,42]

The content of carbon, nitrogen, and hydrogen (CHN) in as-isolated powders was determined by means of combustion elemental analysis (see the Supporting Information). However, no evident relationship to the composition of the precursors could be found. Surprisingly, the determined content of CHN was considerably smaller than expected from the residual mass determined in TG analysis. This suggested a significant oxygen content in the organic residues on the surface of the nanoparticles, presumably in the form of carboxylate functions, which corresponds to the IR measurements.

Therefore, it is can be concluded that the colloidal stability of the formed ZnO particles is due to the formation of a shell composed of coordinating fragments of the ligand moieties of **1** and **2**. This might also account for the difference in colloidal stability of the previously mentioned dispersions. However, one cannot exclude the fact that part of the organic component is located within the particles (e.g., at the boundaries of the crystallites, which form the "blackberries").

Defect Chemistry. Since the defect chemistry of oxide ceramics is of great importance for potential applications in electronic devices, photoluminescence (PL) spectra were studied. As expected for nanoscale zinc oxide powders, a sharp signal in the ultraviolet (UV) range (exciton emission) and a further broader signal, which might consist of several contributions, in the visible regime were

(39) Sakohara, S.; Tickanen, L. D.; Anderson, M. A. *J. Phys. Chem. B* **1992**, *96*, 11086–11091.
(40) Gerstel, P.; Hoffmann, R. C.; Lipowsky, P.; Jeurgens, L. P. H.; Bill, J.; Aldinger, F. *Chem. Mater.* **2006**, *18*, 179–186.
(41) Wöll, C. *Prog. Surf. Sci.* **2007**, *82*, 55–120.
(42) Noei, H.; Qiu, H.; Wang, Y.; Löffler, E.; Wöll, C.; Muhler, M. *Phys. Chem. Chem. Phys.* **2008**, *10*, 7092–7097.

observed, whereby the latter is related to the defect states in the ceramic.[43−45]

In powders obtained from zinc oximato complex **2**, the exciton peak was well-pronounced and considerably stronger than the defect signal (see Figure 10a). The latter consisted clearly of two contributions, i.e., an emission at ∼575 nm ("green") and a second peak at ∼740 nm ("red"). Higher precursor concentrations lead to a weaker "green" emission, in comparison to the intensity of the exciton emission. All signals were subjected to a small blue shift for lower precursor concentrations.

In contrast to these findings, PL spectra of the aforementioned particles from the reaction of **2** in amines exhibited different features. Although the particles did not vary much in size (i.e., in the range of 4−6 nm), the relative intensity of the exciton peak to the visible emission signal was heavily dependent on the reaction temperature. Furthermore, no contribution in the red regime of the spectrum was reported at all.[38]

Spectra of powders obtained from zinc acetylacetonato complex **1** (Figure 10b) showed explicitly different features than those obtained from **2**. The exciton peak was also observable but was always less intense than the signal in the visible range. The latter had only one obvious contribution, with a maximum at ∼530−550 nm. As previously discussed, all signals were subjected to a small blue shift for lower precursor concentrations, indicating a decrease in the crystallite size with the concentration, which is in accordance with the XRD results shown in Tables 1 and 2.

For further processing, it is also noteworthy that defect type and concentration can be influenced drastically by an additional heat treatment. For ZnO powders from both precursor systems, a significant change of position and relative intensity of all signals was observed (see Figures 5 and 6 in the Supporting Information). At temperatures of 250−350 °C, the signals in the visible range showed a distinct increase and descended again at 500 °C. This corresponds with investigations concerning multicolor contributions to the visible luminescence, which is dependent on the calcination atmosphere and temperature. The relative increase and shift of the broad visible signal was discussed relative to changes in the lattice vancancies or interstitials, as well as to a loss of surface hydroxylation of particles or films.[46,47] At temperatures above 450 °C, sintering of the nanoparticles occurred, leading to grain growth and thereby to a reduction of the number of surface defects.[48]

Since our synthesis route allows access to ZnO nanoparticles with a narrow size distribution, the possibility of studying size-selective effects on the defect chemistry seems possible. Further characterization of the defect structure in particles of different sizes derived from **2** was performed using EPR measurements (see Figure 11). To allow more-quantitative conclusions, the size of the particles, as well as the size of the crystallites of the nanosized ZnO, was determined by means of DLS and XRD, respectively (Table 3 in Supporting Information).

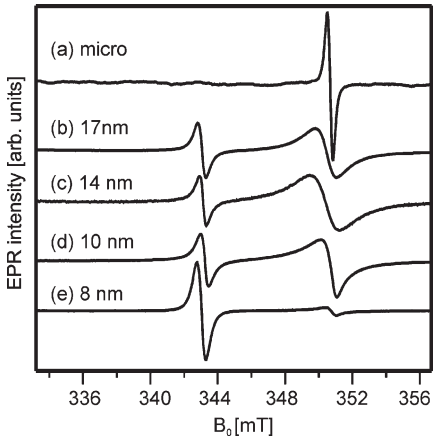

Figure 11. X-band (9.31 GHz) EPR spectra of ZnO powders with different mean particle sizes measured at room temperature: commercial powder, micrometer-sized crystallites (spectrum a) and particles from microwave reaction (spectra b−e). (The latter spectra use a nomenclature scheme of solvent, concentration of oximate precursor, crystallite size (agglomerate size): (b) butoxyethanol, 5%, 17 nm (99 nm); (c) ethoxyethanol, 10%, 14 nm (75 nm); (d) methoxyethanol, 10%, 10 nm (68 nm), and (e) methoxyethanol, 5%, 8 nm (47 nm).

For comparison, a spectrum of a commercially available zinc oxide sample with micrometer-sized particles was also investigated (see Figure 11a). This sample should exhibit more bulk character, in comparison to the nanoparticles with a significantly larger surface-to-volume ratio. The spectrum of the micrometer-sized particles consists of a single resonance at $g = 1.9604$ (∼351 mT), whereby the origin is controversially discussed.[49−51] Because of the complex defect chemistry of zinc oxide singly ionized oxygen defects,[52,53] shallow donor states in the band gap,[54,55] interstitials and zinc vacancies[56,57], or, more generally, multiple defects or defect complexes[58] are proposed. The line shape of the resonance is of Lorentzian type, indicating isolated electrons in the impurity band[59] and ruling out the formation of defect complexes.

(43) Behera, D.; Acharya, B. S. *J. Lumin.* **2008**, *128*, 1577–1586.
(44) Van Dijken, A.; Meulenkamp, E. A.; Vanmaekelbergh, D.; Meijerink, A. *J. Lumin.* **2000**, *87−89*, 454–456.
(45) Van Dijken, A.; Meulenkamp, E. A.; Vanmaekelbergh, D.; Meijerink, A. *J. Lumin.* **2000**, *90*, 123–128.
(46) Djurisic, A. B.; Leung, Y. H.; Hsu, Y. F.; Ding, L.; Ge, W. K.; Zhong, Y. C.; Wong, K. S.; Chan, W. K.; Tam, H. L.; Cheah, K. W.; Kwok, W. M.; Phillips, D. L. *Nanotechnology* **2007**, *18*, 095702.
(47) Djurisic, A. B.; Leung, Y. H.; Tam, K. H.; Ding, L.; Ge, W. K.; Chen, H. Y.; Gwo, S. *Appl. Phys. Lett.* **2006**, *88*, 103107.
(48) Wang, J. M.; Gao, L. *J. Am. Ceram. Soc.* **2005**, *88*, 1637–1639.
(49) Meyer, B. K.; Alves, H.; Hofmann, D. M.; Kriegseis, W.; Forster, D.; Bertram, F.; Christen, J.; Hoffmann, A.; Strassburg, M.; Dworzak, M.; Haboeck, U.; Rodina, A. V. *Phys. Status Solidi B* **2004**, *241*, 231–260.
(50) Evans, S. M.; Giles, N. C.; Halliburton, L. E.; Kappers, L. A. *J. Appl. Phys.* **2008**, *103*, 043710.
(51) Janotti, A.; De Walle, C. G. V. *Phys. Rev. B* **2007**, *76*, 165202.
(52) Hu, Y.; Chen, H. J. *J. Nanopart. Res.* **2008**, *10*, 401–407.
(53) Ischenko, V.; Polarz, S.; Grote, D.; Stavarache, V.; Fink, K.; Driess, M. *Adv. Funct. Mater.* **2005**, *15*, 1945–1954.
(54) Kakazey, M.; Vlasova, M.; Dominguez-Patino, M.; Dominguez-Patino, G.; Sreckovic, T.; Nikolic, N. *Sci. Sinter.* **2004**, *36*, 65–72.
(55) Whitaker, K. M.; Ochsenbein, S. T.; Polinger, V. Z.; Gamelin, D. R. *J. Phys. Chem. C* **2008**, *112*, 14331–14355.
(56) Pöppl, A.; Völkel, G. *Phys. Status Solidi A* **1989**, *115*, 247–255.
(57) Pöppl, A.; Völkel, G. *Phys. Status Solidi A* **1991**, *125*, 571–581.
(58) Djurisic, A. B.; Choy, W. C. H.; Roy, V. A. L.; Leung, Y. H.; Kwong, C. Y.; Cheah, K. W.; Rao, T. K. G.; Chan, W. K.; Lui, H. T.; Surya, C. *Adv. Funct. Mater.* **2004**, *14*, 856–864.
(59) Carlos, W. E.; Glaser, E. R.; Look, D. C. *Physica B* **2001**, *308*, 976–979.

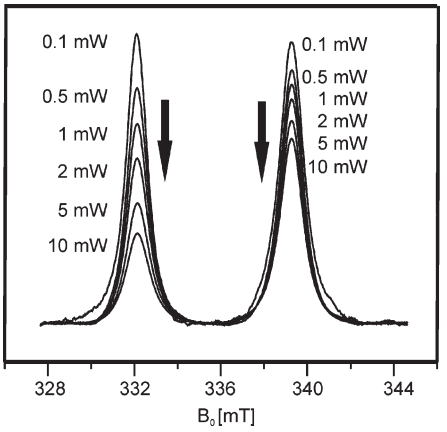

Figure 12. Absorption X-band EPR spectra of a nanosized ZnO powder;[7] the corresponding microwave power is listed beside each peak.

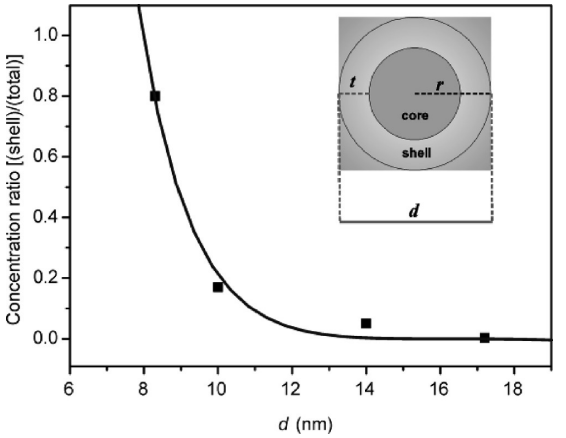

Figure 13. Variation of surface-to-volume ratio for the defect concentrations in ZnO nanopowders, as obtained from the EPR analysis. The solid curve represents a numerical fit to eq 1, based on a core−shell model. The inset schematically illustrates the arrangement assumed for the core−shell model.

For the nanoscale zinc oxide particles, two main aspects in EPR spectra became evident. First, the resonance at $g = 1.9604$ is markedly broadened and the line shape is transformed into a Gaussian shape, indicating hopping of nonisolated electrons to the impurity band. This observation supports the general finding that, in nanosized materials, the defect concentration increases considerably. Moreover, for the smallest crystallites sizes investigated here (i.e., 8 nm), the resonance for the bulk defect almost vanishes. A second feature is the occurrence of a further resonance at $g = 2.0043$ (~343 mT), which is attributed to surface defects.[50] Again, the origin of this defect center is currently under debate. Conceivable candidates are F^+-centers,[60] Zn^- centers,[61] trapped holes (O^-),[62] or O^{2-} superoxide ions formed by the oxygen from (OH) or (C═O) on the surface of the ZnO particles.[52] Contrary to the defect center at $g = 1.9604$, the surface defect has a Lorentzian line shape at nanosizes. This observation is characteristic for a situation in which the defects are highly isolated, such that no defect associates are present. The two individual signals can be modified by UV-light excitation and water absorption.[7]

To investigate the dynamic properties of the two different defect centers, the microwave saturation dependence was studied, as illustrated in Figure 12. Obviously, the saturation behavior of surface signal is much more pronounced, compared to the bulk signal. This observation can be explained by different mobilities of the corresponding electrons at the defect sites. The electrons at the defect centers in the zinc oxide bulk are rather delocalized, and, hence, the corresponding transition are difficult to saturate. On the other hand, electrons trapped at surface defects are considerably more confined, restricting their mobility. Because of the corresponding low electric surface conductivity, the EPR signal is relatively easy to saturate. This is also consistent with the Lorentzian line shape, because isolated defect centers have comparatively long spin−spin relaxation times, increasing the saturation behavior. With regard to the (semi)conducting properties of films that consist of nanoscale zinc oxide, these findings suggest that such surface defects do not contribute to the electron transport, but, instead, inhibit it by means of providing screening charges.[4,5,63]

Because EPR is a local-probe technique, where, mainly, the first coordination sphere of the defect centers influences the resonance lines, the crystallites (within the "blackberries") may be seen as individual objects with electronically distinguishable surface and bulk regions that can be separated from each other, rather than as an interrelated assembly. The overall situation should be comparable to a thin film that consists of nanoscale grains.[7] Therefore, the obtained EPR results may be analyzed, in terms of a core−shell model, where the signal at $g = 1.9604$ originates from the *core* ("*bulk*") and the signal at $g = 2.0043$ originates from the *shell* (surface). Particularly, the paramagnetic susceptibility, as obtained from the EPR experiments, is proportional to the corresponding defect concentrations in core and shell of the nanosized particles. In Figure 13, the concentration ratio between defects at the surface, $[D]_{shell}$, as compared to the total defect concentration, $[D]_{total} = [D]_{bulk} + [D]_{shell}$, is plotted as a function of the mean particle size. Obviously, the defect surface-to-volume ratio increases with reduced mean particle size.

To determine the surface thickness, the following ratio is evaluated by assuming a vanishing defect-concentration gradient over the zinc oxide crystallites:

$$\frac{V_{shell}}{V_{total}} = \frac{3d^2t + 12dt^2 - 8t^3}{d^3} \propto \frac{[D]_{shell}}{[D]_{total}} \qquad (1)$$

where d is the mean crystallite size (values are given in Table 3 in the Supporting Information) and t is the thickness of the surface layer (shell). V_{shell} is the area

(60) Yu, B. L.; Zhu, C. S.; Gan, F.; Huang, Y. B. *Mater. Lett.* **1998**, *33*, 247–250.
(61) Kakazey, N. G.; Sreckovic, T. V.; Ristic, M. M. *J. Mater. Sci.* **1997**, *32*, 4619–4622.
(62) Moribe, S.; Ikoma, T.; Akiyama, K.; Zhang, Q. W.; Saito, F.; Tero-Kubota, S. *Chem. Phys. Lett.* **2007**, *436*, 373–377.
(63) Hu, Y.; Liu, Y.; Li, W.; Gao, M.; Liang, X.; Li, Q.; Peng, L. M. *Adv. Funct. Mater.* **2009**, *19*, 2380–2387.

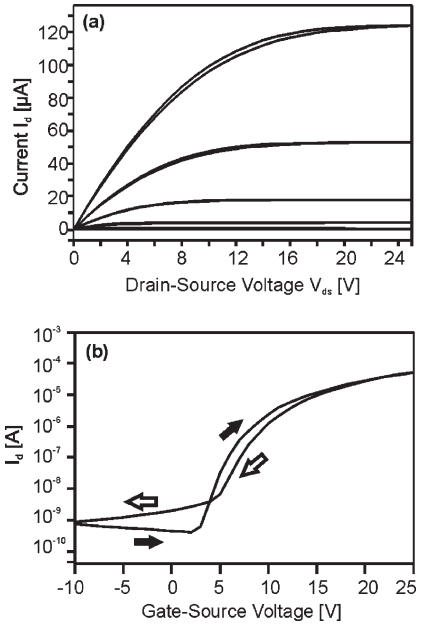

Figure 14. (a) Output characteristic obtained from variation of the drain-source voltage of 0−25 V for gate-source voltages of 0−25 V in steps of 5 V. Data were acquired for increasing as well as decreasing drain-source voltage. (b) Transfer characteristics for a constant drain-source voltage of 25 V. Arrows indicate development of the curve with increasing and decreasing gate-source voltage. A carrier charge mobility of 0.045 cm^2/(V s) was extracted, with an on/off ratio of ~460.000 and $V_{threshold}$ = 8.78 V.

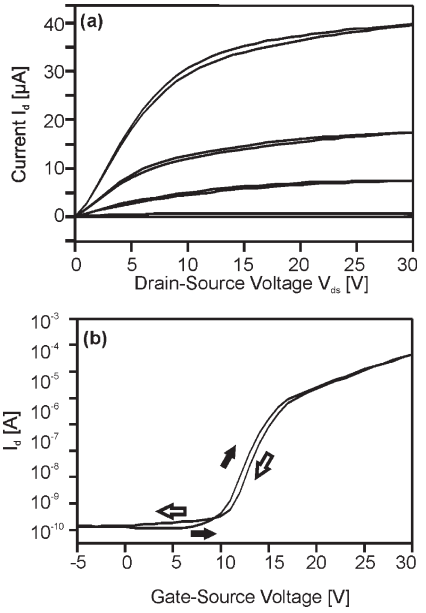

Figure 15. Output characteristic obtained from variation of the drain-source voltage of 0−30 V for gate-source voltages for 0−30 V in steps of 5 V. Data were acquired for increasing (as well as decreasing) drain-source voltages. (b) Transfer characteristic for a constant drain-source voltage of 30 V. Arrows indicate the development of the curve with increasing (and decreasing) gate-source voltage. A carrier charge mobility of 0.010 cm^2/(V s) was extracted, with an on/off ratio of ~630.000 and $V_{threshold}$ = 14.76 V.

obtained from the doubly integrated EPR signal at g = 2.0043, whereas V_{total} is obtained by the double integration of the complete EPR spectrum. After least-squares fitting of the experimental data to eq 1, a thickness of the surface layer for ZnO is determined to 1.000 ± 0.025 nm.

Field-Effect Transistor Device Properties. ZnO thin films obtained via the spin-coating of ZnO particles were obtained from **2** by microwave heating in methoxyethanol on substrates with structured electrodes.[6] (A schematic cross section of the bottom gate/bottom contact device can be found in Figure 7 in the Supporting Information.) Although as-synthesized particles did not show a significant performance, subsequent heating in argon at 250 °C for 10 min, followed by 325 °C for 1 min, leads to a significant improvement in the morphology and the electronic characteristics of the resulting films. (SEM micrographs can be found in Figure 8 in the Supporting Information.) A typical output and transfer characteristic is shown in Figure 14. A carrier charge mobility of 0.045 cm^2/(V s) was extracted, with an on/off ratio of ~460.000 and $V_{threshold}$ = 8.78 V. An alternative treatment of the ZnO particles with UV irradiation under ambient conditions and subsequent heating at 200 °C for 1 min in argon also leads to a comparable FET characteristic with even slightly lower carrier charge mobilities of 0.01 cm^2/(V s), with an on/off ratio of ~630.000 and $V_{threshold}$ = 14.8 V (see Figure 15). These findings are in accordance with the EPR results, which indicate a depletion layer at the surface that provides screen charges. The removal of adsorbed oxygen species from the surface of ZnO in FETs by heating, vacuum treatment, or UV irradiation has been demonstrated by several groups.[63,64] Furthermore, it was shown that the irradiation of ZnO at shorter wavelengths (< 350 nm) not only removed adsorbed molecules, but also prevented a strong chemisorption of oxygen thereafter.[65]

Although the sintering of chalcogenide nanoparticles, which included a rearrangement of the surrounding organic shell, was described for temperatures of > 350 °C,[66,67] no evidence was found for such a process in the previously mentioned samples. However, one cannot totally exclude the possibility that sintering occurs to some extent in samples calcined at 325 °C.

There are several reports demonstrating the field-effect properties of semiconducting ZnO particles in FET devices. However, the required processing and the performance of such devices vary significantly.[6−19] Recently, Halik et al. claimed charge carrier mobilities as high as 2.5 cm^2/(V s) for ZnO nanoparticles 5 nm in diameter, stabilized with an organic shell of 1 nm, which were dried at 80 °C.[15] For sonochemically synthesized ZnO nanoparticles, charge carrier mobilities up to 0.68 cm^2/(V s) and on/off ratios of ~68.000 were reported, remarkably without any further processing (e.g., drying).[16] Hahn et al. reported on FET device performances by dispersing commercially available ZnO nanparticles by means of a copolymeric stabilizing agent and calcining this composite material at 150 °C. However, the mobilities remained

(64) Verma, V. P.; Jeon, H.; Hwang, S.; Jeon, M.; Choi, W. *IEEE Trans. Nanotechnol.* **2008**, *7*, 782–786.
(65) Li, Q. H.; Gao, T.; Wang, Y. G.; Wang, T. H. *Appl. Phys. Lett.* **2005**, *86*, 123117.
(66) Steckel, J. S.; Coe-Sullivan, S.; Bulovic, V.; Bawendi, M. G. *Adv. Mater.* **2003**, *15*, 1862–1866.
(67) Law, M.; Luther, J. M.; Song, Q.; Hughes, B. K.; Perkins, C. L.; Nozik, A. J. *J. Am. Chem. Soc.* **2008**, *130*, 5974–5985.

at $< 10^{-2}$ $cm^2/(V\ s)$, even after optimization.[17,18] This suggests that in situ generation of ZnO particles directly in dispersion might be more advantageous for obtaining higher charge carrier mobilities. Ludwigs et al. described the use of organometallic precursors for ZnO and could remove almost all organic residues by drying under vacuum. However, the performance of FETs obtained in this way remained surprisingly low, i.e., with charge carrier mobilities of $< 10^{-4}$ $cm^2/(V\ s)$.[19]

Several groups have successfully used sol−gel processes (alone or in combination with chemical bath deposition), but in all of these cases, calcination steps in the temperature range of 450−600 °C are required, which are certainly too high for printing applications (e.g., on flexible substrates).[8−14]

Conclusion

The thermal decompostion of zinc acetylacetonato and zinc oximato complexes **1** and **2**, respectively, in alkoxyethanols by microwave heating lead to stable suspensions of nanoscale zinc oxide particles. The employed precursors and solvents, as well as the resulting products, were easy to handle. Although suspensions obtained from **1** were only slightly stable against sedimentation, dispersions derived from **2** were storable for weeks without obvious changes. Such particles consist of an inorganic core and an organic shell. The particle core was built up by several aggregated zincite crystallites, i.e., "blackberry structure". The inorganic core was further surrounded by an organic shell, which consisted of residues of the ligands of the precursors but not of fragments derived from the solvent. The modification of the surface by such organic groups seems to be decisive for the stability of the suspensions against flocculation. The mechanism for the formation of monodisperse colloids with narrow size distribution is well-investigated.[68−70] Because our investigations were in accordance with these findings, only a short outline will be given. In a first stage, primary particles are formed simultaneously in a burst (Le Mer mechanism). The final size of these primary particles is a diffusion-controlled process. In a second stage, the formation of secondary particles occurs (i.e., agglomerates are formed by the primary particles).[68−70] Under the conditions employed here, this aggregation found to be irreversible.

In principle, particles obtained from the decomposition of (**2**) can be employed as semiconductors in FET devices. However, a thermal processing step of ∼325 °C or UV irradiation is required. As suggested by the EPR measurements, as-synthesized particles exhibit a strong surface charge depletion layer caused by adsorption of oxygen on the ZnO surface presumably in the form of O^{2-} ions. These surface defects can be eliminated by the additional treatment. Because of the local sensing mechanism of such defect structures, EPR seems a valuable probe technique for the understanding of electronic properties of ceramic-based semiconductor materials.

Acknowledgment. The support of Prof. Stefan Weber (Universität Freiburg) to R.-A.E., E.E., and P.J. is gratefully acknowledged. TEM measurements were made possible by the Ernst Ruska Zentrum, Forschungszentrum Jülich (Prof. J. Meyer, Dr. L. Houben, and Dr. A. Lysberg) (under the cooperation project ERC1-TUD).

Supporting Information Available: Additional figures and tables (PDF). This material is available free of charge via the Internet at http://pubs.acs.org.

(68) Park, J.; Privman, V.; Matijevic, E. *J. Phys. Chem. B* **2001**, *105*, 11630–11635.
(69) Privman, V.; Goia, D. V.; Park, J.; Matijevic, E. *J. Colloid Interface Sci.* **1999**, *213*, 36–45.
(70) Matijevic, E. *Colloid J.* **2007**, *69*, 29–38.